The Effect of Alongshore Topographic Variation and Bottom Friction on Shelf Wave Interactions

FRANÇOIS W. PRIMEAU* AND GORDON E. SWATERS

Applied Mathematics Institute, Department of Mathematics, University of Alberta, Edmonton, Alberta, Canada

(Manuscript received 19 November 1992, in final form 24 August 1993)

ABSTRACT

The theory of resonant interactions between continental shelf waves developed by Hsieh and Mysak to explain aspects of the shelf wave spectra observed on the Oregon shelf by Cutchin and Smith and Huyer et al. is extended to include the effect of bottom friction and alongshore topographic variation. The model equations are derived via a multiple-scale asymptotic expansion in which it is assumed that the alongshore topography varies over a length scale over which the nonlinear interactions make an order-one contribution to the dynamics. It is shown that alongshore topographic variability leads to a wavenumber mismatch in the wave resonance conditions. It is possible to identify a purely linear and nonlinear component to the wavenumber mismatch. The linear component can be identified simply as the topographic modulation in a WKB sense of the alongshore wavenumber. The nonlinear component of the wavenumber mismatch is a cumulative effect associated with the dynamic interactions between the waves occurring over regions of alongshore topographic variability. It is shown that even after a triad of initially maximally interacting shelf waves has traversed a topographic anomaly of finite alongshore extent, the energy exchange remains permanently suppressed and does not recover to its pretopographic efficiency. For some specialized alongshore topographic variations, the interaction equations can be solved exactly. An illustrative solution is presented for an isolated topographic feature superimposed on an Adams–Buchwald exponential shelf profile. Numerical solutions are presented for the purely dissipative wave interaction problem. For realistic values of the bottom friction parameter it is possible to almost completely damp out any interaction. It is suggested that the geographically localized nature of observed interacting shelf waves may in part be due to alongshore topographic detuning of the resonance conditions or strong frictional effects.

1. Introduction

Motivated by the appearance of three distinct peaks in the coherence spectra of sea level observed on the Oregon shelf by Cutchin and Smith (1973), Hsieh and Mysak (1980) developed a model for the resonant interaction of continental shelf waves. It is well known that wave–wave interactions can occur in dispersive wave systems provided the dispersion relationship admits certain resonance conditions. Hsieh and Mysak showed that an exponential profile model for the Oregon shelf allowed for the resonant interaction of a triad of shelf waves. In particular, it could be shown that the shelf wave spectra observed by Cutchin and Smith, and as well as by Huyer et al. (1975), satisfied the derived resonance conditions. Hsieh and Mysak suggested that the Oregon spectra corresponded to the resonant interaction of a large-scale atmospherically forced shelf wave with two smaller-scale shelf waves.

This was an important and interesting conclusion if for no other reason than the fact that if it is true, the Cutchin and Smith spectra are one of the very few in situ oceanographic observations of large-scale nonlinearly interacting waves. In some respects this conclusion is surprising because of the delicate nature of the required resonance conditions on the frequencies and wavenumbers for interaction. Since the dispersion relationship for freely propagating shelf waves is determined by the shelf profile and this profile varies along the coast it is reasonable to conclude, that as a resonantly interacting packet of continental shelf waves propagates along a shelf, topographically induced phase modulation will lead to a violation of the resonance conditions and consequently a cessation of wave–wave energy exchange. A variety of external forces can be responsible for the modulation of the energy exchange such as topographic irregularities, bottom friction, density stratification and atmospheric forcing. The principal purpose of this paper is to extend the Hsieh and Mysak wave–wave interaction model to include alongshore topographic variations and bottom friction and to describe the role these forces play in modulating

* Current affiliation: WHOI-MIT Joint Program, Department of Earth, Atmospheric and Planetary Sciences, Massachusetts Institute of Technology, Cambridge, Massachusetts.

Corresponding author address: Dr. Gordon E. Swaters, Applied Mathematics Institute, Department of Mathematics, University of Alberta, 632 Central Academic Building, Edmonton, Alberta, Canada T6G 2G1.

the energy exchange in a trio of interacting continental shelf waves.

The wave–wave interaction equations will be derived using the multiple-scale asymptotic expansion procedure introduced by Hsieh and Mysak appropriately modified to take into account alongshore topographic variability and bottom friction. Implicit in the model we derive is that the alongshore topographic variability will correspond to small but finite amplitude irregularities that vary over the same length scale for which the nonlinear terms make an order-one contribution to the dynamics. In addition, it will be assumed that bottom friction makes a significant contribution to the dynamics over the same length scale. These approximations will unfortunately reduce the general applicability of the model but are necessary if, to leading order, the solutions to the governing equations are to correspond to undamped, freely propagating continental shelf waves that are not being continuously and rapidly scattered and damped as the energy propagates along the coast.

The interaction equations will be identical to those presented in Hsieh and Mysak except for two additional terms in each amplitude evolution equation corresponding to the effects alongshore topographic variation and bottom friction. We will show that, roughly speaking, it is possible to identify a *linear* phase and amplitude modulation and an inherently *nonlinear* phase and amplitude modulation associated with these external forcings. The linear response is exactly what one would expect in that the alongshore topographic variability induces a slowly varying modulation of the alongshore wavenumbers in the fast phases associated with each wave packet.

The linear response associated with the damping is also exactly what one would expect in that friction acts to induce a slow exponential decay in each of the wave amplitudes. The nonlinearity in the interaction equations acts to accelerate the decay process. It turns out that the friction coefficients in the nonlinear interaction equations have an inverse dependence on the packet phase speeds. This in turn will imply that short shelf waves will damp out at a faster rate than comparatively longer shelf waves. This fact may be important in the evolution of the triad observed on the Oregon shelf because this ensemble of waves corresponded to the interaction of one long shelf wave with two short shelf waves. Depending on the actual value of the local bottom friction parameter, the decay time scale of the observed triad could range from 0.5 days to 16.4 days. The decay time scale of 0.5 days is far too fast to allow for any substantial energy exchange between the waves, which based on our calculations is about 9 days. The slower decay time scale of about 16.4 days does allow for about two complete cycles of energy exchange. These points are illustrated with a numerical solution of the frictional interaction equations.

The nonlinear response associated with the variable orography is, however, somewhat qualitatively different. To make our description concrete consider the situation in which no friction is present and an orographic irregularity occurs only over a finite alongshore distance. In the linear situation (for which no energy exchange is occurring), there will be a phase modulation of each wave packet *only over the region of alongshore topographic variability.* Thus, once the wave packets have traversed the region of topographic variability (in the sense of following the group velocities), the linear theory would necessarily predict that the spectral characteristics of each wave packet (i.e., the frequencies and wavenumbers) would be identical to those observed prior to encountering the finite region of topographic variability. Consequently, the linear theory would suggest that if a group of continental shelf waves encountered a region of finite alongshore topographic variability, the underlying phases would be modulated only over this region, and in the "downstream" (in the sense of the group velocity) region the spectral characteristics of the wave group would be identical to the "upstream" phases. We will show, however, that the *nonlinear interactions* between the waves over a region of alongshore topographic variability will induce a *permanent* phase modulation in each wave that will result in a permanent reduction in the efficiency of the energy exchange cycle between the waves. Consequently, if a group of maximally interacting continental shelf waves encounters a region of topographic variability, the nonlinear interactions over this region will induce a permanent phase shift in the waves, so that even in the downstream region the wave resonance conditions are detuned to the degree that the energy exchange is permanently suppressed but not necessarily completely eliminated. The degree of suppression is a function of the amplitude of the topographic irregularity and the underlying spectral characteristics of the individual wave packets. These points are illustrated with an exact solution that we can obtain to the inviscid, topographically forced interaction equations for a "top hat" orographic anomaly.

The plan of this paper is as follows. In section 2 the perturbed wave–wave interaction equations are derived. In section 3 we discuss the conservation of energy associated with the interaction equations. In section 4 the various parameters needed in the model are computed using the shelf model introduced by Hsieh and Mysak (1980). In section 5 we present our solutions to the dissipative and topographically forced interaction equations and discuss the implications for shelf wave interactions. Section 6 summarizes the paper and points out some shortcomings in our model and further issues that need to be resolved.

2. Derivation of the governing equations

Hsieh and Mysak (1980) derived the unforced triad equations using the method of multiple scales. Since

this method is well known, and since our method of derivation will closely follow that given by Hsieh and Mysak (except to point out explicitly the modifications brought about by including bottom friction and also alongshore topographic variation), our presentation will be relatively brief. To focus directly on the effects of alongshore topographic variation and bottom friction on the nonlinear wave–wave interactions, we will work with the shallow-water equations on an f plane with Rayleigh bottom friction.

The *nondimensional* nonlinear barotropic long-wave equations for a rigid-lid rotating system with Rayleigh bottom friction are

$$u_t + \varepsilon(uu_x + vu_y) - v = -\eta_x - \varepsilon ru, \quad (2.1)$$

$$v_t + \varepsilon(uv_x + vv_y) + u = -\eta_y - \varepsilon rv, \quad (2.2)$$

$$(hu)_x + (hv)_y = 0, \quad (2.3)$$

where t is time, x and y are, respectively, the offshore and alongshore coordinates; (u, v) are the horizontal velocity components in the (x, y) direction, respectively, η the sea surface displacement from equilibrium (or equivalently the dynamic pressure), and h the water depth. The reader is referred to Hsieh and Mysak (1980) for a complete discussion of the scalings assumed. The dimensionless parameters appearing in (2.1) and (2.2) are the Rossby number given by

$$\varepsilon \equiv U/(Lf), \quad (2.4)$$

where U, L, and f are the horizontal velocity scale, horizontal length scale, and constant Coriolis parameter, respectively, and the bottom friction parameter

$$r \equiv L\tau^{-1}/U, \quad (2.5)$$

where τ is the *dimensional* e-folding time associated with the Rayleigh drag.

Hsieh and Mysak (1980) estimated that the Rossby number, which plays the role of a nondimensional amplitude parameter in (2.1) and (2.2) has magnitude approximately given by $\varepsilon \approx 10^{-2}$ associated with the Oregon data. The nondivergence approximation used in the continuity equation (2.3) will filter out the Poincaré and Kelvin wave modes in the model focusing attention on the relatively lower frequency continental shelf wave solutions. There is a degree of variability in estimating the magnitude of the nondimensional damping coefficient r in (2.1) and (2.2). Assuming Ekman layer dynamics, it follows that r can be estimated from $\tau \approx H_0/(2A_v f)^{1/2}$, where H_0 is the mean depth of the shelf and A_v is a representative vertical turbulent eddy viscosity. Assuming typical values (Hsieh and Mysak 1980) of $L \approx 100$ km, $H_0 \approx 200$ m, $U \approx 10$ cm s^{-1} and $f \approx 10^{-4}$ s^{-1} leads to a range of values for r of approximately 0.7 to 25.0 corresponding to a range of values of A_v of 10^3 cm^2 s^{-1} to 1 cm^2 s^{-1} (Pedlosky 1987, Section 4.2). In what follows we formally assume $0 < \varepsilon \ll 1$ and $r \approx O(1)$ corresponding to weakly nonlinear and dissipative dynamics.

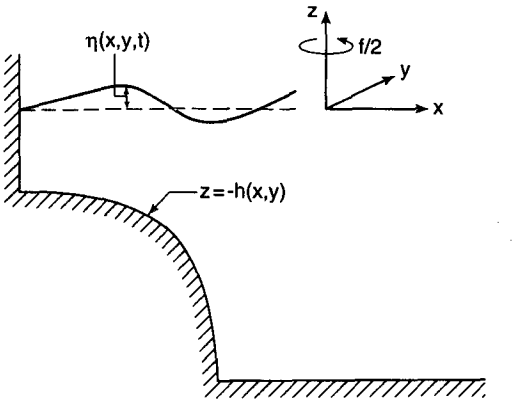

FIG. 1. Geometry of the shallow-water model used in this paper.

The vorticity equation for (2.1) and (2.2) is given by

$$(u_y - v_x)_t + \varepsilon[(uv_x + uv_y)_y - (uv_x + vv_y)_x] - (v_y + u_x) = -\varepsilon r(u_y - v_x). \quad (2.6)$$

Introduction of the transport streamfunction ψ defined by

$$hu = \psi_y, \quad hv = -\psi_x, \quad (2.7)$$

into (2.6) leads to, after a little algebra,

$$h[\psi_{xxt} + \psi_{yyt}] - h_x[\psi_{xt} - \psi_x] - h_y[\psi_{yt} + \psi] + \varepsilon\Big\{r(h\psi_{xx} + h\psi_{yy} - h_x\psi_x - h_y\psi_y) + \left(\frac{h_{xy}}{h} - \frac{3h_xh_y}{h^2}\right)\psi_x^2 + \left(\frac{3(h_x^2 - h_y^2)}{h^2} - \frac{(h_{xx} + h_{yy})}{h}\right)\psi_x\psi_y - \left(\frac{h_{xy}}{h} - \frac{3h_yh_x}{h^2}\right)\psi_y^2 - \frac{2h_y}{h}\psi_y\psi_{yy} + \frac{3h_y}{h}\psi_x\psi_{yy} - \frac{h_y}{h}\psi_y\psi_{xy} + \frac{h_x}{h}\psi_x\psi_{xy} - \frac{3h_x}{h}\psi_y\psi_{xx} + \frac{2h_y}{h}\psi_x\psi_{xx} + \psi_y\psi_{xyy} - \psi_x\psi_{yyy} - \psi_x\psi_{yxx} + \psi_y\psi_{xxx}\Big\} = 0, \quad (2.8)$$

to which we impose the usual boundary conditions for continental shelf waves: namely, that the waves be trapped near the coast, $\psi \to 0$ as $x \to \infty$, and the condition of no mass flux through the coast, $hu = 0$ at $x = 0$, which translates to $\psi_y = 0$ at $x = 0$ on account of (2.7).

The presence of the $O(\varepsilon)$ nonlinear and dissipation terms in (2.8) will lead to a modulation of the leading-order continental shelf wave solutions over an $O(\varepsilon^{-1})$ time and length scale. Accordingly, we introduce the *slow* space and time variables

$$\left.\begin{aligned} Y &= \varepsilon y \\ T &= \varepsilon t \end{aligned}\right\}. \tag{2.9}$$

Consequently, (y, t) derivatives in (2.8) will be rewritten

$$\left.\begin{aligned} \partial_y &\to \partial_y + \varepsilon\partial_Y \\ \partial_t &\to \partial_t + \varepsilon\partial_T \end{aligned}\right\}. \tag{2.10}$$

We shall assume the shelf profile can be expressed in the form

$$h(x, y, Y) = h_0(x) + \varepsilon h_1(x, Y). \tag{2.11}$$

The term $h_0(x)$ in (2.11) corresponds to a cross-shelf depth profile that is uniform in the alongshore direction. The term $\varepsilon h_1(x, Y)$ in (2.11) will correspond to a small-but-finite amplitude variation in the shelf profile. The dependence of $h_1(x, Y)$ on the slow space variable Y implies that the alongshore variation occurs over the same long space scale as the nonlinear energy exchanges. This representation for $h(x, y, Y)$ is forced on us if we wish to examine a dynamical balance between orographic forcing and the wave–wave interactions.

With the introduction of the above variables and shelf profile a uniformly valid asymptotic solution to (2.8) can be obtained in the form

$$\psi(x, y, t) \approx \psi^{(0)}(x, y, Y, t, T) + \varepsilon\psi^{(1)}(x, y, Y, t, T) + O(\varepsilon^2). \tag{2.12}$$

Substitution of (2.9) through to (2.15) into (2.8) yields the $O(1)$ and $O(\varepsilon)$ problems given by

$$O(1): \begin{cases} h_0(\psi^{(0)}_{xxt} + \psi^{(0)}_{yyt}) + h_0'(\psi^{(0)}_y - \psi^{(0)}_{xt}) = 0, \\ \psi^{(0)} \to 0 \quad \text{as} \quad x \to \infty, \\ \psi^{(0)} = 0 \quad \text{at} \quad x = 0, \end{cases} \tag{2.13a, b, c}$$

and

$$O(\varepsilon): \begin{cases} h_0[\psi^{(1)}_{xxt} + \psi^{(1)}_{yyt}] + h_0'[\psi^{(1)}_y - \psi^{(1)}_{yt}] = r(h_0\psi^{(0)}_{xx} + h_0\psi^{(0)}_{yy} - h_0'\psi^{(0)}_x) - h_0[\psi^{(0)}_{xxT} + \psi^{(0)}_{yyT} + 2\psi^{(0)}_{yYt}] \\ \quad + h_0'[\psi^{(0)}_{xT} - \psi^{(0)}_Y] + \left[\frac{h_0''}{h_0} - \left(\frac{h_0'}{h_0}\right)^2\right]\psi^{(0)}_x\psi^{(0)}_y + \frac{3h_0'}{h_0}\psi^{(0)}_{xx}\psi^{(0)}_y - \frac{h_0'}{h_0}\psi^{(0)}_x\psi^{(0)}_{xy} - \psi^{(0)}_{xxx}\psi^{(0)}_y + \psi^{(0)}_x\psi^{(0)}_{xxy} \\ \quad + \frac{2h_0'}{h_0}\psi^{(0)}_{yy}\psi^{(0)}_y - \psi^{(0)}_{xyy}\psi^{(0)}_y + \psi^{(0)}_x\psi^{(0)}_{yyy} - h_1[\psi^{(0)}_{yyt} - \psi^{(0)}_{xxt}] - h_{1x}[\psi^{(0)}_y - \psi^{(0)}_x], \\ \psi^{(1)} \to 0 \quad \text{as} \quad x \to \infty, \qquad \psi^{(0)}_Y + \psi^{(1)}_y = 0 \quad \text{at} \quad x = 0, \end{cases} \tag{2.14a, b, c}$$

where for convenience prime denotes d/dx.

The $O(1)$ equations, being linear and not including any topographic forcing or any damping, permit a solution consisting of the superposition of three freely propagating continental shelf waves in the form

$$\psi^{(0)} = \sum_{j=1}^{3} A_j(Y, T)\phi(x)\exp(i\theta_j) + \text{c.c.}, \tag{2.15}$$

where the amplitudes $A_j(Y, T)$ are slowly varying functions of alongshore position and time, the fast phases are $\theta_j = k_j y - \omega_j t$, $i^2 = -1$ and c.c. denotes complex conjugate. Substitution of (2.15) into (2.13) leads to the Sturm–Liouville problem

$$\left.\begin{aligned} -\left(\frac{-1}{h_0}\phi_j'\right)' + \frac{(-k_j^2)}{h_0}\phi_j - \frac{1}{c_j}\left(\frac{h_0'}{h_0^2}\right)\phi_j = 0 \\ \phi_j(x) \to 0 \quad \text{as} \quad x \to \infty \\ \phi(0) = 0 \end{aligned}\right\}, \tag{2.16a, b, c}$$

where the reciprocal of the phase speed $c_j^{-1} = k_j/\omega_j$ is the eigenvalue.

Substitution of (2.15) into (2.14a) allows the $O(\varepsilon)$ problem to be expressed in the form

$$h_0[\psi^{(1)}_{xxt} + \psi^{(1)}_{yyt}] + h_0'[\psi^{(1)}_{y} - \psi^{(1)}_{xt}]$$
$$= \sum_{j=1}^{3} \left(\frac{-h_0'}{c_j} \phi_j A_{jT} - (h_0' + 2k_j\omega_j h_0)\phi_j A_{jY} + (rh_0\phi_j'' - rh_0k_j^2\phi_j - rh_0'\phi_j' - ih_{1}\omega_j k_j\phi_j + ih_{1}\omega_j\phi_j'' - ik_j h_{1_x}\phi_j \right.$$
$$\left. + i\omega_j h_{1_x}\phi_j')A_j \right) \exp(i\theta_j) + \sum_{l=1}^{3}\sum_{m=1}^{3} \left[\frac{-2h_0'}{h_0} k_l^2\phi_l\phi_m + \left(\frac{h_0''}{h_0} - 3\left(\frac{h_0'}{h_0}\right)^2 + k_l^2 - k_m^2 \right)\phi_l'\phi_m + \frac{3h_0'}{h_0}\phi_l''\phi_m \right.$$
$$\left. - \frac{h_0'}{h_0}\phi_l'\phi_m' - \phi_l'''\phi_m \right] \left[ik_m A_l A_m \exp(i\theta_l + i\theta_m) - ik_m A_l A_m^* \exp(i\theta_l - i\theta_m) \right] + \text{c.c.}, \quad (2.17)$$

where (2.16) has been used and where the asterisk denotes complex conjugation.

The required wave–wave interaction equations are obtained by exploiting certain solvability conditions associated with (2.17). We begin by observing that the frequencies and wavenumbers on the left-hand side must match those on the right-hand side. Thus the contribution of the particular solution to $\phi^{(1)}$ must be of the form

$$\psi^{(1)} = \sum_{\alpha} \tilde{A}_\alpha(Y, T)\tilde{\phi}_\alpha(x) \exp(i\theta_\alpha) + \text{c.c.} \quad (2.18)$$

We shall assume that the three waves in (2.15) from a resonant triad satisfying the well-known resonance conditions (without loss of generality)

$$\left.\begin{aligned} k_1 + k_2 + k_3 &= 0 \\ \omega_1 + \omega_2 + \omega_3 &= 0 \end{aligned}\right\}. \quad (2.19a, b)$$

Hsieh and Mysak (1980) have shown that for a Buchwald and Adams (1968) and Adams and Buchwald (1969) exponential shelf profile, the Sturm–Liouville problem (2.16) admits dispersion relationships for which such resonant triads can in fact exist. In Fig. 2 we show the triad used by Hsieh and Mysak to model the Cutchin and Smith spectra. Under the resonance conditions (2.19), it follows that the fast phase in the explicitly written out quadratic interaction term in (2.17) has the form $\theta_p = \theta_l \pm \theta_m$, where p is an integer from the set $\{1, 2, 3\}$ different from l and m. Thus, the phase θ_α in (2.18) must necessarily be of the form

$$\{\theta_\alpha\} = \{\theta_j | j = 1, 2, 3\} \cup \{\theta_l \pm \theta_m | l = 1, 2, 3 \text{ and } m = 1, 2, 3\}. \quad (2.20)$$

Substituting (2.18) into the left-hand side of (2.17) we find that for each j, $\phi_j^{(1)}$ must satisfy an inhomogeneous equation of the form

$$-\left(\frac{-1}{h_0}\phi_j^{(1)\prime}\right)' + \frac{-k_j^2}{h_0}\phi_j^{(1)} - \frac{1}{c_j}\left(\frac{h_0'}{h_0^2}\right)\phi_j^{(1)} = f_j, \quad (2.21)$$

where f_j denotes the forcing at frequency ω_j and wavenumber k_j from the right-hand side of (2.17). The Fredholm alternate theorem from Sturm–Liouville theory (see, e.g., Boyce and Diprima 1969, p. 506) states that the inhomogeneous problem (2.21) has a solution $\phi_j^{(1)}$ only if the forcing term f_j is orthogonal to the homogeneous solutions ϕ_j; that is,

$$\int_0^\infty f_j\phi_j dx = 0, \quad (2.22)$$

for *each* $j = 1, 2, 3$. Consequently, the solvability condition (2.22) requires that

$$(\partial_T + c_{g_1}\partial_Y)A_1 = -iK_1A_2^*A_3^* - r_1A_1 - i\mu_1(Y)A_1,$$
$$(\partial_T + c_{g_2}\partial_Y)A_2 = -iK_2A_3^*A_1^* - r_2A_2 - i\mu_2(Y)A_2,$$
$$(\partial_T + c_{g_3}\partial_Y)A_3 = -iK_3A_1^*A_2^* - r_3A_3 - i\mu_3(Y)A_3, \quad (2.23a, b, c)$$

corresponding to $j = 1, 2, 3$, respectively, in (2.22) and where we have normalized the ϕ_j so that

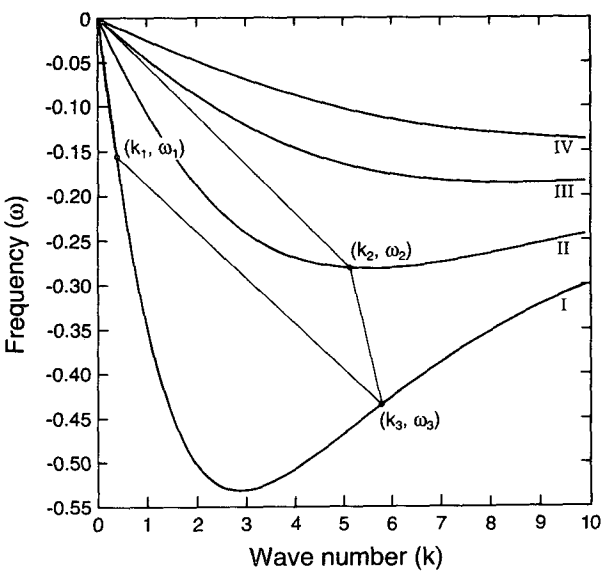

FIG. 2. The resonant triad used by Hsieh and Mysak (1980) to model the Cutchin and Smith shelf wave spectra. The curves labeled I, II, III, and IV correspond to the four lowest modes associated with the Buchwald–Adams shelf profile used by Hsieh and Mysak.

$$\int_0^\infty \frac{h_0'}{h_0^2}\phi_j^2 dx = 1, \tag{2.24}$$

for each $j = 1, 2, 3$ and where

$$K_j \equiv c_j(K_{jlm} + K_{jml}), \tag{2.25}$$

is the interaction coefficient where

$$K_{jlm} \equiv \int_0^\infty \frac{k_m}{h_0^2}\left[\frac{-3h_0'}{h_0}\phi_j'\phi_l'\phi_m + 2\phi_j'\phi_l''\phi_m - \frac{2h_0'}{h_0}k_l^2\phi_j\phi_l\phi_m + (k_l^2 - k_m^2)\phi_j\phi_l'\phi_m\right]dx, \tag{2.26}$$

and where

$$c_{g_j} = c_j(1 + \gamma_j c_j k_j^2), \tag{2.27}$$

is the group velocity with

$$\gamma_j = \int_0^\infty \frac{1}{h_0}\phi_j^2 dx, \tag{2.28}$$

and the friction parameters given by

$$r_j \equiv -\frac{r}{c_j}, \tag{2.29}$$

and where

$$\mu_j(Y) \equiv \int_0^\infty dx\left[\omega_j k_j^2 \frac{h_1}{h_0}\phi_j^2 - \omega_j \frac{h_1}{h_0^2}\phi_j''\phi_j + k_j \frac{h_{1_x}}{h_0^2}\phi_j^2 - \omega_j \frac{h_{1_x}}{h_0^2}\phi_j'\phi_j\right] \tag{2.30}$$

is the topography coefficient. For complete details of the derivation see Primeau (1992).

For our subsequent discussion it will be convenient to recast the interaction equations into "standard" form. To this end we define the new amplitude functions $\alpha_j(Y, T)$ given by

$$\alpha_j(Y, T) \equiv A_j(Y, T)\exp[-i\sigma_j(Y)/c_{g_j}], \tag{2.31}$$

where

$$\sigma_j(Y) \equiv \int_0^{\epsilon Y} \mu_j(\xi)d\xi, \tag{2.32}$$

for $j = 1, 2, 3$. Substitution of (2.31) into (2.23) yields the interaction equations in the form

$$(\partial_T + c_{g_1}\partial_Y)\alpha_1 = -iK_1\alpha_2^*\alpha_3^*\exp[-i\sigma_0(Y)] - r_1\alpha_1,$$

$$(\partial_T + c_{g_2}\partial_Y)\alpha_2 = -iK_2\alpha_3^*\alpha_1^*\exp[-i\sigma_0(Y)] - r_2\alpha_2,$$

$$(\partial_T + c_{g_3}\partial_Y)\alpha_3 = -iK_3\alpha_1^*\alpha_2^*\exp[-i\sigma_0(Y)] - r_3\alpha_3, \tag{2.33a, b, c}$$

where

$$\sigma_0(Y) \equiv \frac{\sigma_1(Y)}{c_{g_1}} + \frac{\sigma_2(Y)}{c_{g_2}} + \frac{\sigma_3(Y)}{c_{g_3}}. \tag{2.34}$$

It is now possible to heuristically see the "linear" and "nonlinear" influence the alongshore variation in the shelf profile will have on the waves. The additional phase factored out in (2.31) corresponds to an $O(\varepsilon)$ slowly varying correction to the alongshelf wavenumber given by $\partial_y[-\sigma_j(Y)/c_{g_j}] = -\varepsilon\mu_j(Y)/c_{g_j}$. This response is entirely linear. The *nonlinear* response on the individual packet amplitudes will be determined by the solutions to (2.33). Notice how the topographic inhomogeneities in (2.33) can be interpreted as taking the form of a spatially varying interaction coefficient. As the interacting wave packets enter regions where $\sigma_0(Y) \neq 0$, the spatial dependence of the interaction coefficient will lead to a loss of efficiency of the energy exchange. This effect will lead to both an amplitude and phase modulation that can be identified as purely nonlinear on account of the fact that the linearized form of (2.33) has no topographic inhomogeneities at all. Another point to bring out is that because the spatial dependence in each of the interaction coefficients is identical in (2.33a,b,c), it will be possible to obtain exact topographically forced solutions for some special cases. These are discussed in section 5. Finally, we remark that a similar transformation to (2.31) can be introduced in order to factor out the linearized exponential decay associated with the friction and to introduce an interaction coefficient that will depend on the slow time. However, no further analytical progress can be made with that set of equations since the dependence of the interaction coefficients on the slow time will not be identical in each wave packet and thus it is simply more convenient for our subsequent discussion to work with either (2.23) or (2.33).

3. Conservation of energy

Hsieh and Mysak presented an argument for showing that the wave–wave interactions conserved energy in the absence of topographic forcing and dissipation. We now show that inviscid limit of our interaction equations also possess this property. Of course this is to be expected since the topographic variability should be considered as a conservative force. The argument we present here is somewhat different than that described by Hsieh and Mysak in that we proceed axiomatically from a phase-averaged conservation law approach.

The vorticity equation (2.8) in the inviscid limit can be rewritten in the form

$$\left[\nabla\cdot\left(\frac{1}{h}\nabla\psi\right)\right]_t + J\left[\frac{\varepsilon}{h}\nabla\cdot\left(\frac{1}{h}\nabla\psi\right) - \frac{1}{h}, \psi\right] = 0, \tag{3.1}$$

where $J(A, B) \equiv A_xB_y - A_yB_x$. The energy equation is obtained by multiplying (3.1) by ψ and rearranging terms to yield

$$\left[\frac{1}{2h}\nabla\psi\cdot\nabla\psi\right]_t + \nabla\cdot\left[-\frac{\psi}{h}\nabla\psi_t + (\hat{e}_3\times\nabla\psi)\psi\left(\frac{\varepsilon}{h}\nabla\left(\frac{1}{h}\nabla\psi\right)-\frac{1}{h}\right)\right] = 0. \quad (3.2)$$

The energy equation can be expressed as a conservation law (Pedlosky 1979, section 3.27) in the form

$$E_t + \nabla\cdot\mathbf{F} = 0, \quad (3.3)$$

with

$$E = \frac{1}{2h}\nabla\psi\cdot\nabla\psi, \quad (3.4)$$

$$\mathbf{F} = -\frac{\psi}{h}\nabla\psi_t + \hat{e}_3\times\nabla\psi\psi\left(\frac{\varepsilon}{h}\nabla\left(\frac{1}{h}\nabla\psi\right)-\frac{1}{h}\right), \quad (3.5)$$

as the energy density and flux, respectively. When the perturbation expansion (2.9) through (2.12) is substituted into (3.3), an expression of the form

$$(E_t^{(0)} + F_{1,x}^{(0)} + F_{2,y}^{(0)}) + \varepsilon(E_T^{(0)} + E_t^{(1)} + F_{1,x}^{(1)} + F_{2,Y}^{(0)} + F_{2,y}^{(1)}) + \cdots = 0, \quad (3.6)$$

is obtained. The leading-order energy density and energy flux components are given by

$$E^{(0)} = \frac{1}{2h_0}\nabla\psi^{(0)}\cdot\nabla\psi^{(0)}, \quad (3.7)$$

$$F_1^{(0)} = \frac{\psi_y^{(0)}\psi^{(0)}}{h_0} - \frac{\psi^{(0)}\psi_{xt}^{(0)}}{h_0}, \quad (3.8)$$

$$F_2^{(0)} = -\frac{\psi_x^{(0)}\psi^{(0)}}{h_0} - \frac{\psi^{(0)}\psi_{yt}^{(0)}}{h_0}. \quad (3.9)$$

We now introduce the averaging operator

$$\langle(*)\rangle = \frac{1}{(2\pi)^3}\int_0^\infty\int_0^{2\pi}\int_0^{2\pi}\int_0^{2\pi}(*)d\theta_1 d\theta_2 d\theta_3 dx, \quad (3.10)$$

where $\theta_j = k_j y - \omega_j t, j = 1, 2, 3$ are the phase variables. Note that, if $\langle(*)\rangle$ operates on a function that is periodic with period 2π in any of the phase variables, the average will vanish. If the averaging operator is applied to (3.6) it follows to $O(\varepsilon)$ that

$$\langle E^{(0)}\rangle_T + \langle F_2^{(0)}\rangle_Y = 0. \quad (3.11)$$

This expression will be the appropriate energy conservation law that the interacting shelf waves need to satisfy. Note that all the other $O(1)$ and $O(\varepsilon)$ terms in the averaged (3.6) will be identically zero because of the following reasons: $\langle E_t^{(0)}\rangle = \langle F_{2,y}^{(0)}\rangle \equiv 0$ because of the periodicity of the $O(1)$ solutions; $\langle F_{1,x}^{(0)}\rangle = \langle F_{1,x}^{(1)}\rangle \equiv 0$ on account of the boundary conditions at $x = 0$ and $x = \infty$. It also follows that $\langle E_t^{(1)}\rangle = \langle F_{2,y}^{(1)}\rangle \equiv 0$ because of the periodicity of the $O(1)$ and $O(\varepsilon)$ solutions provided the latter are solely determined by the particular solutions to (2.17), that is, we do not allow any freely propagating shelf wave solutions to the $O(\varepsilon)$ problem. Finally, we note that differentiation with respect to the slow variables commutes with the averaging operator since the integration limits are independent of these arguments. Substitution of the $O(1)$ solution given by (2.15) into (3.7), (3.8), and (3.9) yields, after a little algebra:

$$E^{(0)} = \frac{1}{h_0}(\phi_1'^2 + k_1^2\phi_1^2)|A_1|^2 + \frac{1}{h_0}(\phi_2'^2 + k_2^2\phi_2^2)|A_2|^2 + \frac{1}{h_0}(\phi_3'^3 + k_3^2\phi_3^2)|A_3|^2 + \{\text{terms that will average to zero}\}, \quad (3.12)$$

$$F_2^{(0)} = \frac{1}{h_0}(2|A_1|^2\phi_1'\phi_1 + 2|A_2|^2\phi_2'\phi_2 + 2|A_3|^2\phi_3'\phi_3 - 2k_1\omega_1|A_1|^2\phi_1^2 - 2k_2\omega_2|A_2|^2\phi_2^2 - 2k_3\omega_3|A_3|^2\phi_3) + \{\text{terms that will phase average to zero}\}. \quad (3.13)$$

If (3.12) is averaged, it follows that

$$\langle E^{(0)}\rangle = \int_0^\infty \frac{1}{h_0}[|A_1|^2(\phi_1'^2 + k_1^2\phi_1^2) + |A_2|^2(\phi_2'^2 + k_2^2\phi_2^2) + |A_3|^2(\phi_3'^2 + k_3^2\phi_3^2)]dx. \quad (3.14)$$

Integrating the $h_0^{-1}\phi_j'^2, j = 1, 2, 3$ terms in (3.14) by parts, exploiting (2.16) and the normalization condition (2.24), we obtain

$$\langle E^{(0)}\rangle = -\frac{1}{c_1}|A_1|^2 - \frac{1}{c_2}|A_2|^2 - \frac{1}{c_3}|A_3|^2, \quad (3.15)$$

which is identical to the result presented in Hsieh and Mysak. Similar arguments show

$$\langle F_2^{(0)}\rangle = -\frac{c_{g_1}}{c_1}|A_1|^2 - \frac{c_{g_2}}{c_2}|A_2|^2 - \frac{c_{g_3}}{c_3}|A_3|^2, \quad (3.16)$$

which is also the result presented in Hsieh and Mysak. Thus, the three waves interaction equations will conserve energy provided that

$$[|A_1|^2/c_1 + |A_2|^2/c_2 + |A_3|^2/c_3]_T + [c_{g_1}|A_1|^2/c_1 + c_{g_2}|A_2|^2/c_2 + c_{g_3}|A_3|^2/c_3]_Y = 0 \quad (3.17)$$

holds.

To show that energy is in fact conserved in the inviscid, topographically forced interaction equations, we go back to the form (2.23)

$$\left.\begin{aligned}(\partial_T + c_{g_1}\partial_Y)A_1 &= -iK_1A_2^*A_3^* - i\mu_1(Y)A_1\\ (\partial_T + c_{g_2}\partial_Y)A_2 &= -iK_2A_3^*A_1^* - i\mu_2(Y)A_2\\ (\partial_T + c_{g_3}\partial_Y)A_3 &= -iK_3A_1^*A_2^* - i\mu_3(Y)A_3\end{aligned}\right\}. \quad (3.18)$$

If we multiply the jth equation in (3.18) by $-A_j^*/c_j$, we obtain the following system

$$\left.\begin{aligned}&\frac{-A_1^*}{c_1}(\partial_T + c_{g_1}\partial_Y)A_1\\ &\qquad = \frac{iK_1}{c_1}A_1^*A_2^*A_3^* + \frac{i\mu_1(Y)}{c_1}|A_1|^2\\ &\frac{-A_2^*}{c_2}(\partial_T + c_{g_2}\partial_Y)A_2\\ &\qquad = \frac{iK_2}{c_2}A_1^*A_2^*A_3^* + \frac{i\mu_2(Y)}{c_2}|A_2|^2\\ &\frac{-A_3^*}{c_3}(\partial_T + c_{g_3}\partial_Y)A_3\\ &\qquad = \frac{iK_3}{c_3}A_1^*A_2^*A_3^* + \frac{i\mu_3(Y)}{c_3}|A_3|^2\end{aligned}\right\}. \quad (3.19a, b, c)$$

If the sum (3.19a) + (3.19b) + (3.19c) + c.c. is formed, it follows that

$$\partial_T\left(\frac{1}{c_1}|A_1|^2 + \frac{1}{c_2}|A_2|^2 + \frac{1}{c_3}|A_3|^2\right) + \partial_Y\left(\frac{c_{g_1}}{c_1}|A_1|^2 + \frac{c_{g_2}}{c_2}|A_2|^2 + \frac{c_{g_3}}{c_3}|A_3|^2\right) = 2\,\mathrm{Re}\{iA_1A_2A_3\}\left(\frac{K_1}{c_1} + \frac{K_2}{c_2} + \frac{K_3}{c_3}\right). \quad (3.20)$$

Note that the topographic terms in this sum will add up to identically zero since the topographic terms in (3.19a,b,c) are purely imaginary. It follows from (3.20) and (3.17) that the three wave interactions will conserve energy if and only if

$$\frac{K_1}{c_1} + \frac{K_2}{c_2} + \frac{K_3}{c_3} = 0. \quad (3.21)$$

Hsieh and Mysak showed that (3.21) holds for resonantly interacting shelf waves.

4. The theory applied to an exponential shelf

To proceed further in our study of the topographically forced resonant triad, it is necessary to specify explicitly the cross-shelf profile $h_0(x)$. Hsieh and Mysak (1980) originally developed their wave–wave interaction theory for the Oregon shelf, which they modeled with a Buchwald and Adams (1968) and Adams and Buchwald (1969) exponential shelf profile of the form

$$h_0(x) = \begin{cases} H_1e^{2bx}, & 0 \leqslant x \leqslant 1\\ H_2, & 1 < x < \infty, \end{cases} \quad (4.1)$$

where b, H_1, and H_2 are constant parameters with $H_2 = H_1e^{2b}$. We shall also use this cross-shelf profile.

With the above choice for h_0, the Sturm–Liouville problem (2.16) yields the following dispersion relation for the nth offshore mode (see Buchwald and Adams 1968),

$$\omega_j^{(n)} = -2bk_j/[(\xi_j^{(n)})^2 + k_j^2 + b^2], \qquad n = 1, 2, 3, \cdots, \quad (4.2)$$

where $\xi_j^{(n)}$ is the nth root of the transcendental equation

$$\tan(\xi_j^{(n)}) = -\xi_j^{(n)}/(b + |k_j|), \quad \xi_j^{(n)} > 0. \quad (4.3)$$

The cross-shelf eigenmode $\phi_j^{(n)}(x)$ is given by

$$\phi_j^{(n)}(x) = \begin{cases} N_j^{(n)}\sin(\xi_j^{(n)}x)\exp[b(x-1)], & 0 \leqslant x < 1\\ N_j^{(n)}\sin(\xi_j^{(n)})\exp[-|k_j|(x-1)], & 1 < x < \infty, \end{cases} \quad (4.4)$$

where the constant $N_j^{(n)}$ is evaluated via the normalization condition (2.24) and is found to be given by

$$N_j^{(n)} = [2\xi_j^{(n)}H_2/b(2\xi_j^{(n)} - \sin 2\xi_j^{(n)})]^{1/2}. \quad (4.5)$$

Having obtained explicit expressions for the ϕ_j, we can obtain analytical expressions for the coefficients appearing in the interaction equations (2.23). Substitution of (4.4) into (2.28) yields the following expression for γ_j:

$$\gamma_j \equiv \frac{N_j^2}{H_2}\left[\left(\frac{1}{2} - \frac{\sin(2\xi_j)}{4\xi_j}\right) + \frac{\sin^2(\xi_j)}{2|k_j|}\right], \quad (4.6)$$

which can then be substituted into (2.27) to obtain the group velocities, c_{g_j}. Also, as shown by Hsieh and Mysak (1980), substitution of (4.4) into (2.26) yields the following expressions for the K_{jlm}:

$$K_{jlm} \equiv N_jN_lN_m\frac{1}{H_2^2}k_m \times \Big\{b(-3b^2 - \xi_j^2 - 2\xi_l^2 - 3k_l^2 - 3k_l^2 - k_m^2)I_1 + \xi_l(-b^2 - \xi_j^2 + k_l^2 - k_m^2)I_2 + 2\xi_j(-b^2 - \xi_l^2)I_3 + \frac{\sin(\xi_j)\sin(\xi_l)\sin(\xi_m)}{|k_j| + |k_l| + |k_m|} \times [k_l^2(-2|k_j| - |k_l|) + |k_l|(k_m^2 - k_j^2)]\Big\}, \quad (4.7)$$

where

$$I_1 \equiv \frac{1}{4}[(bA_1 + b_1B_1 - b_1C_1) - (bA_2 + b_2B_2 - b_2C_2) - (bA_3 + b_3B_3 - b_3C_3) + (bA_4 + b_4B_4 - b_4C_4)], \quad (4.8)$$

$$I_2 \equiv = \frac{1}{4}[(b_1A_1 - bB_1 + b_1C_1) - (b_2A_2 - bB_2 + b_2C_2) + (b_3A_3 - bB_3 + b_3C_3) - (b_4A_4 - bB_4 + b_4C_4), \quad (4.9)$$

$$I_3 \equiv \frac{1}{4}[-(b_1A_1 - bB_1 + bC_1) + (b_2A_2 - bB_2 + bC_2) + (b_3A_3 - bB_3 + bC_3) - (b_4A_4 - bB_4 + bC_4)], \quad (4.10)$$

$$\left.\begin{aligned} b_1 &\equiv \xi_j - \xi_l - \xi_m, \quad b_2 \equiv \xi_j - \xi_l + \xi_m \\ b_3 &\equiv \xi_j + \xi_l - \xi_m, \quad b_4 \equiv \xi_j + \xi_l + \xi_m \end{aligned}\right\}, \quad (4.11)$$

and

$$[A_i, B_i, C_i] \equiv \frac{1}{h^2 + b_i^2}[\sin b_i, \cos b_i, e^b], \quad i = 1, 2, 3, 4. \quad (4.12)$$

The K_{jlm} can then be combined via (2.25) to form the interaction coefficients, that is, the K_j appearing in (2.23).

Finally for the special case where h_1 is assumed to be a function of Y only, the integration in the definition of the topography coefficient (2.33) can be explicitly performed to give

$$\mu_j(Y) = h_1(Y)\mu_{j_0}, \quad (4.13)$$

where

$$\mu_{j_0} \equiv \frac{N_j^2\omega_j}{4H_2^2}[(b^2 - k_j^2 - \xi_j^2)/b + e^{2b}(-b^2 + k^2 - z^2)/b + \{be^{2b}(b^2 - k_j^2 - 3\xi_j^2) + b(-b^2 + k_j^2 + 3\xi_j^2) \times \cos(2\xi_j) + \xi_j(3b^2 - k_j^2 - \xi_j^2) \times \sin(2\xi_j)\}/(b^2 + \xi_j^2)]. \quad (4.14)$$

5. Solutions of the interaction equations

a. Some general remarks

For sufficiently smooth $\sigma_0(Y)$, it is known (Craik 1985) that a solution to the initial-value problem for (2.33) uniquely exists for all time provided not all the interaction coefficients K_j are of the same sign. Note that the K_j in the shelf wave theory do possess this property on account of the energy conservation condition (3.21) and the fact that for our model geometry the phase velocities are strictly negative. Not all problems of geophysical interest necessarily have this property. For example, Meacham (1988) has shown that it is possible that the interaction coefficients for baroclinic Rossby waves can be all of the same sign. When this occurs, the initial-value solutions to the interaction equations necessarily become singular in finite time. This solution corresponds to a finite-amplitude, nonmodal instability.

Even though the existence and uniqueness of solutions to our model have been established, there are no known exact solutions for a general topographic function $\sigma_0(Y)$ to either the steady-state or time-dependent interaction equations, even in the absence of damping. Cree and Swaters (1991) examined a topographically forced triad of Rossby wave packets. They showed that when $\sigma_0(Y)$ is a quadratic function with respect to Y it is always possible to transform the interaction equations into a form formally solved using an inverse scattering transform (IST). They also showed how similar transformations could be introduced into the linearized "pump-wave" approximation to the interaction equations. Both of these techniques allow one to examine special initial-value solutions to the wave–wave interaction equations. These methods can be modified in an obvious fashion to apply to the model presented here.

A third method developed by Cree and Swaters can be used to obtain exact nonlinear steady-state solutions when $\sigma_0(Y)$ is a linear function. This solution will be briefly described in section 5.c. In section 5.d we will show how to construct a nonlinear steady-state solution for the interacting waves assuming a top-hat topographic anomaly, which has a finite extent in the alongshore direction. Although this is a crude topographic configuration, the simplicity of the analytic solution serves well in elucidating how alongshore topography acts to "dephase" the resonant interaction.

Finally we note that because the damping coefficients r_j are mutually different, exact solutions cannot, in general, be obtained for the damped problem even for the purely temporal problem in the absence of alongshore topography. Because of this we will present, in the next section, numerical solutions for the purely temporal problem in order to illustrate the balance between energy dissipation and nonlinear energy exchange in the evolution of the packet amplitudes.

b. The purely temporal problem

To focus on the effects of bottom friction and energy exchange, we will look, in this section, at the purely temporal problem with no alongshore topography variation. In the next section, we will study the steady-state problem in which we retain the alongshore topographic variation but neglect the bottom friction.

To study the purely temporal dissipation problem we start with (2.26) and set $\partial_Y \equiv 0$ and $\sigma_0(Y) \equiv 0$. With the above simplifications, (2.23) reduces to

$$\left.\begin{aligned}\frac{dA_1}{dT} &= -iK_1A_2^*A_3^* - r_1A_1\\ \frac{dA_2}{dT} &= -iK_2A_3^*A_1^* - r_2A_2\\ \frac{dA_3}{dT} &= -iK_3A_1^*A_2^* - r_3A_3\end{aligned}\right\}. \tag{5.2.1}$$

If we introduce the transformation

$$A_j(T) \equiv a_j(T)\exp[i\theta_j(T)], \tag{5.2.2}$$

where a_j and θ_j are real functions, into (5.2.1), we obtain the system of real-valued ordinary differential equations

$$\left.\begin{aligned}\frac{da_1}{dT} &= -K_1a_2a_3\sin\theta - r_1a_1\\ \frac{da_2}{dT} &= -K_2a_2a_3\sin\theta - r_2a_2\\ \frac{da_3}{dT} &= -K_3a_1a_2\sin\theta - r_3a_3\end{aligned}\right\}, \tag{5.2.3}$$

$$\left.\begin{aligned}a_1\frac{d\theta_1}{dT} &= -K_1a_2a_3\cos\theta\\ a_2\frac{d\theta_2}{dT} &= -K_2a_3a_1\cos\theta\\ a_3\frac{d\theta_3}{dT} &= -K_3a_1a_2\cos\theta\end{aligned}\right\}, \tag{5.2.4}$$

where $\theta = \theta_1 + \theta_2 + \theta_3$.

To obtain numerical values for the interaction coefficients in the above equations, we will use the Buchwald and Adams exponential shelf profile (4.1) with parameters chosen by Hsieh and Mysak to model the Oregon shelf given by

$$\left.\begin{aligned}b &= 1.65\\ H_1 &= 0.524\\ H_2 &= 14.2\end{aligned}\right\}, \tag{5.2.5}$$

(the horizontal length scale is $L = 112$ km and the shelf depth scale is $H_0 = 200$ m) and the triad used by Hsieh and Mysak given by

$$\left.\begin{aligned}(k_1, \omega_1) &= (0.382, -0.155)\\ (k_2, \omega_2) &= (5.362, -0.281)\\ (k_3, \omega_3) &= (-5.745, 0.436)\end{aligned}\right\}, \tag{5.2.6}$$

(see Fig. 2). With these values for the shelf parameters and the resonant triad substituted into (4.7)–(4.11) and (2.25), we obtain the following numerical values for the interaction coefficients

$$\left.\begin{aligned}K_1 &= -8.757\\ K_2 &= -2.054\\ K_3 &= 4.613\end{aligned}\right\}. \tag{5.2.7}$$

The nondimensional damping parameter r is given by (2.5). If we choose the horizontal velocity scale to be $U = 10^{-1}$ m s^{-1}, and the horizontal length scale to be $L = 112$ km, the numerical values for r range from approximately 0.79 to 25.04 depending on the magnitude of A_V used. Using the upper estimate for r we obtain the following damping coefficients

$$\left.\begin{aligned}r_1 &= 6.90\\ r_2 &= 53.42\\ r_3 &= 36.90\end{aligned}\right\}, \tag{5.2.8}$$

while using the lower estimate for r we obtain

$$\left.\begin{aligned}r_1 &= 0.01\\ r_2 &= 0.05342\\ r_3 &= 0.04\end{aligned}\right\}. \tag{5.2.9}$$

Note that there is quite a range in the magnitude of physically realistic damping parameters for this triad. Since the damping coefficients are mutually different, analytical solutions to (5.2.3) and (5.2.4) cannot be obtained (see Weiland and Wilhelmsson 1977). We note that if $\theta = \pi/2$ or $3\pi/2$ (the case where energy exchange is maximized), (5.2.4) is trivially satisfied for all T, and consequently θ remains constant so that (5.2.3) becomes uncoupled from (5.2.4). In Figs. 3 and 4 we show the decay of the amplitude functions $a_j(T)$ for a maximally interacting triad with $\theta_1 = \theta_2 = \theta_3 \equiv \pi/2$ with the damping parameters given by (5.2.8) and (5.2.9).

While resonant interactions are a possible mechanism for energy exchange when Ekman friction is weak, we can see that strong bottom friction causes an e-folding decay time much smaller than the period of oscillation of the amplitudes, and we can see that unless energy is being pumped into the system by external forcing, such as wind stress, for example, the energy exchange due to nonlinear interactions will be negligible.

To obtain numerical values for the period of oscillation of the amplitudes, we neglect friction in (5.2.3) so that the equations can be solved analytically. Setting $r_j = 0$, $(j = 1, 2, 3)$ and taking $\theta = \pi/2$, the solution to (5.2.3) is, as shown by Hsieh and Mysak (1980), given by Jacobi elliptic functions. Without loss of generality we can choose $T = 0$ to be the instant when $a_1 > 0$, $a_2 > 0$, and $a_3 = 0$. With this choice of initial conditions the solutions are

$$\left.\begin{aligned}a_1(T) &= a_{1_0}dn(\sigma T/M)\\ a_2(T) &= a_{2_0}cn(\sigma T/M)\\ a_3(T) &= a_{1_0}(-K_3/K_2)^{1/2}sn(\sigma T/M)\end{aligned}\right\}, \tag{5.2.11}$$

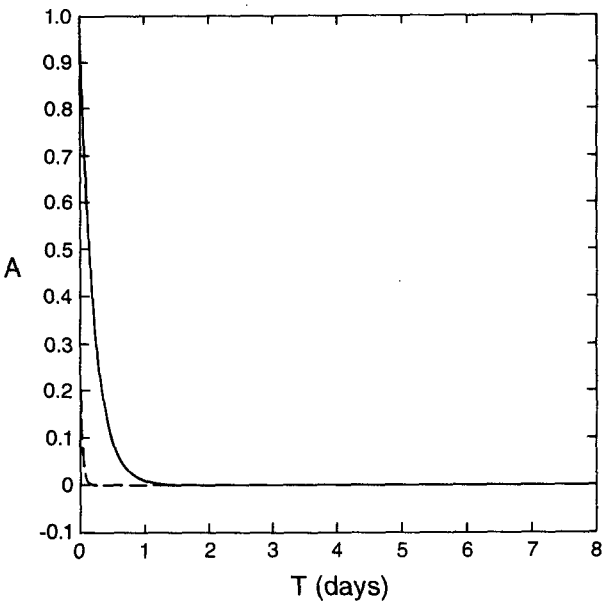

FIG. 3. The effect of bottom friction on a maximally interacting resonant triad of shelf waves for the relatively large damping coefficients given by (5.2.8). The triad corresponds to the Cutchin and Smith data. The solid, dashed, and dotted curves correspond to a_1, a_2, and a_3, respectively.

where

$$\sigma \equiv a_{1_0}(-K_2K_3)^{1/2}, \tag{5.2.12}$$

$$M \equiv K_1 a_{2_0}^2 (K_2 a_{1_0}^2), \tag{5.2.13}$$

and dn, dn, sn are the Jacobi elliptic functions (Abramowitz and Stegun 1965, chapter 16). Without loss of generality we may assume $0 \leq M \leq 1$. The period of energy transfer is given by the period T_d, of the elliptic function $dn(\sigma T/M)$, given by

$$T_d = 2K(M)/\sigma = 2K(M)a_{1_0}^{-1}(-K_2K_3)^{-1/2}, \tag{5.2.14}$$

where $K(M)$ is a complete elliptic integral of the first kind. Using the same parameters and initial conditions ($a_{1_0} = 1$, $a_{2_0} = 0.4$, $a_{3_0} = 0$) used in the numerical solutions, we find $T_d \approx 1.33$. Remembering that t has been nondimensionalized with respect to $1/f$, ($f \approx 10^{-4}\ s^{-1}$) and that $T = \varepsilon t$, where ε is the Rossby number ($\varepsilon \approx 10^{-2}$), it follows that $T_d \approx 17$ days. Hence for the given initial conditions, the time scale of energy transfer ($\sim \frac{1}{2} T_d$) is about 9 days. The e-folding time due to Ekman friction range from 0.5 days to 16.4 days. For the lower estimate of friction, the e-folding time is longer than the period of energy exchange so that some energy can be transferred to the other members of the triad before the waves are damped out. On the other hand, for the upper estimate of friction, the e-folding time is much shorter than the period of energy exchange, and resonant interactions cannot be expected to provide a mechanism for energy exchange between the three wave components. In fact for the upper estimate of friction our perturbation expansion may not be valid and friction may need to be included at first order.

Because the range of estimates in the Ekman number is so large, the theory developed in this paper is inconclusive as to whether resonant interactions are a viable mechanism for resonant energy exchange in the presence of bottom friction. It is quite likely that the magnitude of the Ekman number varies with time and location, and this fact may explain in part why there are so few observations of shelf wave interactions.

c. *Steady-state solution with alongshore topographic variation*

In this section we focus on the effect of alongshore topographic variation on a resonant triad of shelf waves in the inviscid limit in which $r_1 = r_2 = r_3 \equiv 0$ in (2.33). The first point that should be made is that there exist no known exact solutions to the topographically forced interaction equations for an arbitrary topographic profile. In the case with no topographic anomaly, corresponding to $\sigma_0 \equiv 0$, the initial-value problem for the interaction equations has a unique solution, which can be formally obtained using an IST (Kaup et al. 1979). Cree and Swaters (1991) showed how it was possible to transform the topographically forced interaction equations in the special case where $\sigma_0(Y)$ was a quadratic function in the variable Y, back into the form of the unforced interaction equations. The situation

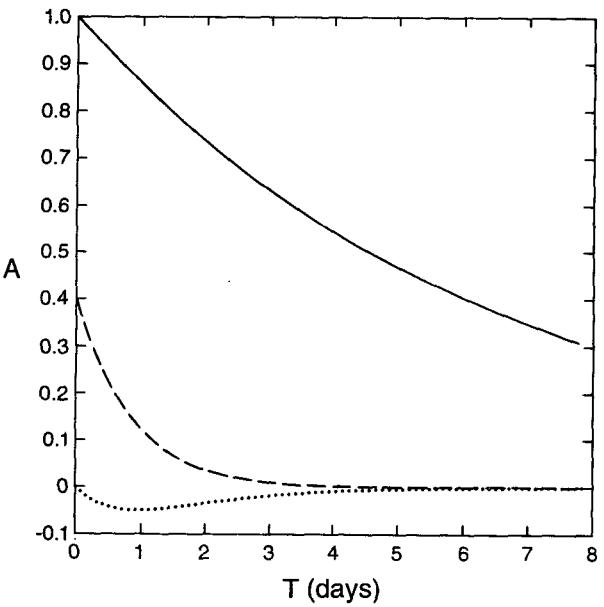

FIG. 4. The effect of bottom friction on a maximally interacting triad of shelf waves for the relatively small damping coefficients given by (5.2.9). The triad corresponds to the Cutchin and Smith data. The solid, dashed, and dotted curves are as described in Fig. 3.

were $\sigma_0(Y)$ is a quadratic function corresponds to a topographic anomaly which is a *linear* function of Y; see (2.32). Thus, at least formally, the complete solution to the initial-value associated with shelf wave interactions over a topographic anomaly which varies linearly in the along-shelf direction can be analytically determined. However, the solution procedure is very complicated and all of the conclusions that we wish to draw can be made by examining the solutions to a simpler but still nontrivial problem. In what follows we describe the exact, nonlinear *steady-state* solutions that can be obtained assuming that the topographic coefficient $\sigma_0(Y)$ is a *linear* function of the alongshore coordinate Y. This solution can be interpreted as the topographically forced analogs of the solutions presented in Hsieh and Mysak. In section 5.d we show how to use the solution constructed here to describe the alongshore spatial structure of interacting shelf waves for a simple topographic anomaly of finite alongshore extent.

For the steady-state ansatz adopted in this section to be physically relevant, we restrict attention to a wave triad in which the individual group velocities are all of the same sign. For such a situation, the direction of energy propagation will be the same for each wave and it will be meaningful to speak of a quasi-steady interaction that "begins" on one side of a region of topographic variability and "proceeds," in the sense of following the group velocities, over the orographic irregularity. If the group velocities are not all of the same sign, the energy associated with the wave packets begins to separate rapidly and the interaction process becomes time-dependent on a O(1) time scale. To make our description concrete we will work with a triad in which the group velocities are all negative; see (5.4.3). It will be obvious how to modify our procedures to handle the situation in which the group velocities are all positive. These points are important because it means that, unfortunately, we are not able to directly apply our topographic results to the specific wave triad modeled by Hsieh and Mysak since that triad was composed of shelf waves which did not all have the same sign for the group velocities (see Fig. 2).

Suppose that the topographic coefficient $\sigma_0(Y)$ in (2.33) has the simple linear form

$$\sigma_0(Y) = \sigma H(Y - Y_s), \tag{5.3.1}$$

where

$$\sigma \equiv \mu_{10}/c_{g_1} + \mu_{20}/c_{g_2} + \mu_{30}/c_{g_3}, \tag{5.3.2}$$

with the μ_{j_0} determined by (4.14) and the c_{g_j} are the respective group velocities. The constant parameters H and Y_s correspond, respectively, to the maximum height of the topographic anomaly and to the alongshore position of zero topographic anomaly. If (5.3.1) is substituted into the interaction equations (2.33), the steady inviscid equations can be written in the form

$$\alpha_{1_\xi} = -iK_{10}\alpha_2^*\alpha_3^* \exp(-i\sigma H\xi), \tag{5.3.3a}$$

$$\alpha_{2_\xi} = -iK_{20}\alpha_1^*\alpha_3^* \exp(-i\sigma H\xi), \tag{5.3.3b}$$

$$\alpha_{3_\xi} = -iK_{30}\alpha_1^*\alpha_2^* \exp(-i\sigma H\xi), \tag{5.3.3c}$$

where $K_{j_0} \equiv K_j/c_{g_j}$ for $j = (1, 2, 3)$ and $\xi \equiv Y - Y_s$.

The solution to (5.3.3) can be found in the form

$$\alpha_j(\xi) \equiv b_j(\xi) \exp[i\Phi_j(\xi)], \tag{5.3.4}$$

for $j = (1, 2, 3)$, where the $b_j(\xi)$ and $\Phi_j(\xi)$ are real-valued functions. The $b_j(\xi)$ and $\Phi_j(\xi)$ will determine the amplitude and phase modulations, respectively, induced by the nonlinear interactions in the presence of variable orography. We remind the reader that the *linear* phase modulation associated with the topographic variation has already been factored out on account of the transformation (2.31). Substitution of (5.3.4) into (5.3.3) yields, after separating real and imaginary parts, the coupled system

$$b_{1_\xi} = K_{10}b_2b_3 \sin(\Phi), \tag{5.3.5a}$$

$$b_{2_\xi} = K_{20}b_3b_1 \sin(\Phi), \tag{5.3.5b}$$

$$b_{3_\xi} = K_{30}b_1b_2 \sin(\Phi), \tag{5.3.5c}$$

$$\Phi_{1_\xi} = -K_{10}(b_2b_3/b_1) \cos(\Phi), \tag{5.3.6a}$$

$$\Phi_{2_\xi} = -K_{20}(b_1b_3/b_2) \cos(\Phi), \tag{5.3.6b}$$

$$\Phi_{3_\xi} = -K_{30}(b_1b_2/b_3) \cos(\Phi), \tag{5.3.6c}$$

where

$$\Phi \equiv -\Phi_1 - \Phi_2 - \Phi_3 - \sigma H\xi. \tag{5.3.7}$$

It follows from (5.3.6) and (5.3.7) that

$$\Phi_\xi = -\sigma H + b_1b_2b_3(K_{10}/b_1^2 + K_{20}/b_2^2 + K_{30}/b_3^2) \cos(\Phi). \tag{5.3.8}$$

The solutions are most easily obtained by simultaneously solving (5.3.5) and (5.3.8) and then determining the individual Φ_j's by substituting the b_j's and Φ into (5.3.6) and integrating.

It is possible to see qualitatively how topography acts to dephase the wave–wave interactions based on (5.3.5), (5.3.6), and (5.3.7). It follows from (5.3.5) that maximum energy exchange occurs for $\sin(\Phi) = \pm 1$ or equivalently $\Phi = \pm(2n + 1)\pi/2$ [consequently $\cos(\Phi) = 0$], where n is a nonnegative integer. We may assume, without loss of generality, that initially $\Phi_1 = \Phi_2 = \Phi_3 = \pi/2$ corresponding to a maximally interacting triad. In the absence of any alongshore topographic variation (i.e., $H = 0$), it will follow from (5.3.8) that Φ remains equal to $-3\pi/2$ thereafter and thus from (5.3.6) it follows that $\Phi_1 = \Phi_2 = \Phi_3 = \pi/2$ for all ξ. In addition, from (5.3.5) it follows that the energy exchange will remain maximized because $\sin(\Phi) = -1$. On the other hand if $\sigma H \neq 0$ in (5.3.8),

then $\Phi_\xi \neq 0$ initially and the change in water depth will act to induce a nonzero Φ and thus, on account of (5.3.6), the envelope phases will have magnitudes that will diverge from their initial values. Also, as Φ moves away from $-3\pi/2$, the interaction coefficients in (5.3.5) will reduce in magnitude and the energy exchange will no longer be maximized.

To obtain the solution to (5.3.5) and (5.3.8) for $\sigma H \neq 0$ we proceed as follows. First, we introduce the normalizations

$$b_1 = |K_{20}K_{30}|^{-1/2}\hat{b}_1, \tag{5.3.9a}$$

$$b_2 = |K_{30}K_{10}|^{-1/2}\hat{b}_2, \tag{5.3.9b}$$

$$b_3 = |K_{10}K_{20}|^{-1/2}\hat{b}_3. \tag{5.3.9c}$$

Substitution of (5.3.9) into (5.3.5) and (5.3.7) yields

$$\hat{b}_{1\xi} = s_1\hat{b}_2\hat{b}_3 \sin(\Phi), \tag{5.3.10a}$$

$$\hat{b}_{2\xi} = s_2\hat{b}_3\hat{b}_1 \sin(\Phi), \tag{5.3.10b}$$

$$\hat{b}_{3\xi} = s_3\hat{b}_1\hat{b}_2 \sin(\Phi), \tag{5.3.10c}$$

$$\Phi_\xi = -\sigma H + \hat{b}_1\hat{b}_2\hat{b}_3(s_1/\hat{b}_1^2 + s_2/\hat{b}_2^2 + s_3/\hat{b}_3^2)\cos(\Phi), \tag{5.3.11}$$

where $s_j = \text{sgn}(K_{j0})$ with $j = 1, 2, 3$. It follows immediately from energy conservation and the fact that the group velocities are all assumed to be negative, that two of the K_{j0} are of one sign and the other differs in sign, and because of this, two of the s_j are of one sign while the other differs in sign. Without loss of generality we can choose $s_2 = s_3 = 1$ and $s_1 = -1$.

There are several constants of motion associated with (5.3.10) and (5.3.11). If the products $\hat{b}_1 \times$ (5.3.10a), $\hat{b}_2 \times$ (5.3.10b) and $\hat{b}_3 \times$ (5.3.10c) are formed and the results integrated with respect to ξ over the interval (ξ_0, ξ) it follows that

$$[\hat{b}_1^2(\xi) - \hat{b}_1^2(\xi_0)] = -[\hat{b}_2^2(\xi) - \hat{b}_2^2(\xi_0)] = -[\hat{b}_3^2(\xi) - \hat{b}_3^2(\xi_0)], \tag{5.3.12}$$

for all ξ and ξ_0 assuming our choice for the s_j. These are the Manley–Rowe relations (Craik 1985) for (5.3.10). It will be convenient for our future work to introduce the auxiliary dependent variable

$$\hat{y}(\xi) = -[\hat{b}_1^2(\xi) - \hat{b}_1^2(\xi_0)], \tag{5.3.13}$$

which on account of the Manley–Rowe relations will imply $\hat{y}(\xi) = \hat{b}_j^2(\xi) - \hat{b}_j^2(\xi_0)$ for $j = 2, 3$.

Another quantity that will be convenient for our subsequent work is the constant of motion given by

$$\Gamma \equiv \hat{b}_1\hat{b}_2\hat{b}_3 \cos(\Phi) + \sigma H\hat{b}_1^2/2. \tag{5.3.14}$$

To show that Γ is a constant of the motion it is sufficient to show $\Gamma_\xi = 0$. This can be done by taking the derivative of the left- and right-hand sides of (5.3.14) with respect to ξ eliminating the $\hat{b}_{j\xi}$ and Φ_ξ using (5.3.10) and (5.3.11), respectively.

To proceed further we derive an ordinary differential equation for $\hat{y}(\xi)$. If (5.3.9b) is multiplied by $\hat{b}_2(\xi)$, it follows that

$$(\hat{b}_3^2)_\xi = \pm 2\{\hat{b}_1^2\hat{b}_2^2\hat{b}_3^2[1 - \cos^2(\Phi)]\}^{1/2}. \tag{5.3.15}$$

Now, if (5.3.13) and the Manley–Rowe relations are used to eliminate the $\hat{b}_j^2$ terms and (5.3.14) is used to eliminate the $\cos^2(\Phi)$ term, it follows that

$$\frac{1}{2}\left(\frac{\partial \hat{y}}{\partial \xi}\right)^2 + p(\hat{y}) = 0, \tag{5.3.16}$$

where

$$p(\hat{y}) \equiv -2\left\{[\hat{b}_1^2(\xi_0) - \hat{y}][\hat{b}_2^2(\xi_0) + \hat{y}][\hat{b}_3^2(\xi_0) + \hat{y}] - \left[\Gamma - \frac{\sigma H}{2}(\hat{b}_1^2(\xi_0) - \hat{y})\right]^2\right\}. \tag{5.3.17}$$

The polynomial $p(\hat{y})$ is cubic in the dependent variable $\hat{y}(\xi)$. Equation (5.3.16) can be thought of as describing the motion of a particle in a nonlinear potential well determined by $p(\hat{y})$. In this viewpoint, the "coordinate" $\hat{y}$, giving the position of the particle, is proportional to the deviation of the squared values of the wave amplitudes from their initial values. We also note that only the range of $\hat{y}$ for which $p(\hat{y}) \leq 0$ has any physical significance, and $\partial\hat{y}/\partial\xi = 0$ when $p(\hat{y}) = 0$. It is possible to show (Weiland and Wilhelmsson 1977; Craik 1985) that because not all the s_j coefficients in (3.1.8) have the same sign (which followed from energy conservation), $p(\hat{y})$ will have three real roots denoted $\hat{y}_1$, $\hat{y}_2$, and $\hat{y}_3$ satisfying, without loss of generality, the ordering $\hat{y}_1 > \hat{y}_2 > \hat{y}_3$. The solution $\hat{y}(\xi)$ will, in general, oscillate between the two largest roots of $p(\hat{y})$.

In terms of these roots, (5.3.16) can be rewritten in the form

$$(\hat{y}_\xi)^2 = -4(\hat{y} - \hat{y}_1)(\hat{y} - \hat{y}_2)(\hat{y} - \hat{y}_3). \tag{5.3.18}$$

The solution of (5.3.18) is given by the cnoidal function $\text{sn}(*|*)$ (Abramowitz and Stegun 1964, chapter 17 in the form

$$\hat{y} = (\hat{y}_2 - \hat{y}_1)\,\text{sn}^2[\pm(\hat{y}_1 - \hat{y}_3)^{1/3}(\xi - \xi_0) + \hat{\theta}|\hat{k}] + \hat{y}_1, \tag{5.3.19a}$$

where

$$\hat{k} \equiv [(\hat{y}_1 - \hat{y}_2)/(\hat{y}_1 - \hat{y}_3)]^{1/2}, \tag{5.3.19b}$$

$$\hat{\theta} \equiv \text{sn}^{-1}\{[\hat{y}_1/(\hat{y}_1 - \hat{y}_2)]^{1/2}\}, \tag{5.3.19c}$$

are the modulus and shift parameters, respectively. The solution (5.3.19a) is periodic with respect to ξ with a wavelength, denoted λ_I, given by

$$\lambda_I = 2\int_0^{2\pi} [1 - \hat{k}\sin^2(\xi)]^{-1/2} d\xi.$$

The parameter λ_I determines the alongshore distance over which the energy exchange undergoes one complete cycle.

With the solution for $\hat{y}(\xi)$ determined the modulated amplitudes are given by

$$\hat{b}_1(\xi) = \pm[\hat{b}_1^2(\xi_0) - \hat{y}(\xi)]^{1/2}, \quad (5.3.20a)$$

$$\hat{b}_2(\xi) = \pm[\hat{b}_2^2(\xi_0) - \hat{y}(\xi)]^{1/2}, \quad (5.3.20b)$$

$$\hat{b}_3(\xi) = \pm[\hat{b}_3^2(\xi_0) - \hat{y}(\xi)]^{1/2}. \quad (5.3.20c)$$

The solution for $\Phi(\xi)$ may be obtained by eliminating $\hat{b}_1\hat{b}_2\hat{b}_3 \cos(\Phi)$ in (5.3.11) using (5.3.14) and integrating to yield

$$\Phi(\xi) = \Phi(\xi_0) - \sigma H(\xi - \xi_0) + \int_{\xi_0}^{\xi} [\Gamma - \sigma H\hat{b}_1^2(\eta)/2] \times [-\hat{b}_1^{-2}(\eta) + \hat{b}_2^{-2}(\eta) + \hat{b}_3^{-2}(\eta)]d\eta. \quad (5.3.21)$$

Similarly, the individual envelope phases are determined by

$$\Phi_1(\xi) = \Phi_1(\xi_0) - \int_{\xi_0}^{\xi} \frac{[2\Gamma - \sigma H\hat{b}_1^2(\eta)]}{2\hat{b}_1^2(\eta)} d\eta, \quad (5.3.22a)$$

$$\Phi_2(\xi) = \Phi_2(\xi_0) - \int_{\xi_0}^{\xi} \frac{[2\Gamma - \sigma H\hat{b}_1^2(\eta)]}{2\hat{b}_2^2(\eta)} d\eta, \quad (5.3.22b)$$

$$\Phi_3(\xi) = \Phi_3(\xi_0) - \int_{\xi_0}^{\xi} \frac{[2\Gamma - \sigma H\hat{b}_1^2(\eta)]}{2\hat{b}_3^2(\eta)} d\eta. \quad (5.3.22c)$$

d. Interactions over a topographic anomaly of finite alongshore extent

The solution obtained in section 5.c can be used as a "building block" in understanding orographically modulated shelf wave interactions that occur over topographic anomalies of finite alongshore extent. The topographic perturbation that we examine is given by

$$h_1 = \begin{cases} 0, & Y_0 < Y < 0 \\ \bar{H}, & Y_1 < Y < Y_0 \\ 0, & -\infty < Y < Y_1. \end{cases} \quad (5.4.1)$$

This topographic perturbation corresponds to a top-hat anomaly extending over a distance $|Y_0 - Y_1|$ in the alongshore direction (see Fig. 5). Although this top-hat configuration is extremely crude, it will rather nicely allow us to draw out the main conclusion we can make about the model.

There are a couple of remarks we should make about the anomaly model (5.4.1) before moving on to presenting the solution. Clearly, h_1 corresponds to a topographic anomaly possessing an $O(\varepsilon)$ amplitude finite step discontinuity at $Y = Y_1$ and $Y = Y_0$, respectively; see (2.11). Thus, strictly speaking, the topographic slowly varying ansatz implicit in (2.11) is violated at these two locations. Formally, therefore, the modulated

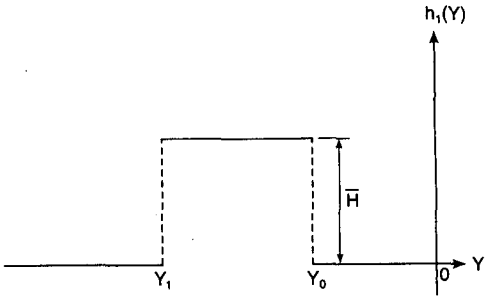

FIG. 5. The top-hat alongshore topographic anomaly assumed in section 5.d.

$O(1)$ solutions we present here will correspond to "outer solutions," which correctly describe the leading-order streamfunction everywhere except possibly in two relatively narrow regions centered at $Y = Y_1$ and $Y = Y_0$, respectively. Because, as it turns out, we can determine these "outer solutions" in such a manner so as to satisfy all boundary conditions and the continuity of pressure and normal mass flux across $Y = Y_1$ and $Y = Y_0$, respectively, the solutions we obtain will be the correct *leading-order* asymptotic solutions as $\varepsilon \to 0$. However, if one were interested in determining the complete $O(\varepsilon)$ streamfunction field, the details of the transmission of the wave groups across these discontinuities plays an important role in the analysis. Roughly speaking, the $O(\varepsilon)$ problem (2.14) should be viewed as an inhomogeneous shelf-wave scattering problem in which it is to be expected that a full spectrum of coastally trapped waves will be required in order to correctly describe the complete scattering and transmission of energy across $Y = Y_1$ and $Y = Y_0$, respectively. These additional modes would introduce small amplitude $O(\varepsilon)$ corrections into the solution.

It is also important to emphasize again that the specific shelf wave triad and topographic anomaly configuration we examine here obviously corresponds to a rather special set of initial conditions. From the point of view of wanting to realistically simulate all aspects of topographically modulated shelf–wave interactions, one would want to numerically solve the full initial-value problem for the wave–wave interaction equations. Clearly, there will be a relatively large number of possible solutions determined, in part, by the initial envelope shapes and specific orographic forcing. For example, in the situation where the initial envelope shapes have smooth compact support, it is well known (e.g., Kaup et al. 1979), that, qualitatively, the unforced solution evolves into a combination of envelope solitons and dispersive waves. If the topographic forcing in the interaction equations is relatively weak and smooth, then soliton perturbation theory (e.g., Kaup and Newell 1978) would qualitatively suggest that these individual envelope solitons would, to leading order, modulate adiabatically with the possibility of dispersive wave tails being generated. If the topographic forcing

in the wave–wave interaction equations is not weak, then soliton perturbation theory is not naively appropriate. The situation being considered here belongs to the latter configuration in which the topographic anomaly makes an O(1) contribution to the wave–wave interaction equations. With respect to an explicit mathematical characterization of the initial wave envelopes assumed here, they are members of the set of steady or steadily traveling periodic cnoidal wave solutions of the unforced interaction equations.

The solution for the topographically forced interaction equations can be obtained as follows. Since we are working with shelf waves that have negative group velocities we will impose our "initial" conditions to the right of the topographic feature, that is, at $Y = 0$. In each individual Y interval, $Y_0 < Y$, $Y_1 < Y < Y_0$, and $Y < Y_1$, the solution will be of the form derived in section 5.c for an appropriately determined shift parameter Y_s and jump parameter H. Since, in general, the Y_s parameter will be different for the individual regions, the auxiliary independent variable ξ used in the solutions presented in section 5.3 will be different for the individual Y intervals in (5.4.1). Nevertheless, the solutions for the envelope amplitude and phase functions can be made continuous at the Y interval boundaries (i.e., Y_0 and Y_1) by choosing the initial values of the b_j of the interval just entered, to the final values of the amplitudes of the region just exited. One then recomputes the new roots $\hat{y}_1$, $\hat{y}_2$, and $\hat{y}_3$ of the polynomial (5.3.17) with the new initial values of the b_j and topographic parameters. The parameter ξ_0 in (5.3.19a) then determined so the new $\hat{y}$ satisfies $\hat{y}(\xi_0) = 0$ at the Y interval boundary point just passed. Also, at each Y interval boundary point, one must determine which sign is appropriate for the argument of sn in (5.3.19a). The correct sign is chosen so that when the rhs of (5.3.10a) is positive at the boundary point then $\hat{b}_1$ must be increasing to the left of the boundary point, and vice versa if the rhs is negative. Forcing $\hat{b}_1$ to be increasing or decreasing will fix the correct sign for sn's argument in (5.3.19a).

For the top-hat anomaly (5.4.1), the parameters and arguments Y_s, ξ, ξ_0, and H needed in the solution will be given by

$$\left.\begin{aligned} Y_s &= 0 \\ \xi &= Y \\ H &= 0 \\ \xi_0 &= 0 \end{aligned}\right\} \quad \text{in} \quad Y_0 \leqslant Y \leqslant 0, \qquad (5.4.2a)$$

$$\left.\begin{aligned} Y_s &= Y_0 \\ \xi &= Y - Y_0 \\ H &= \bar{H} \\ \xi_0 &= 0 \end{aligned}\right\} \quad \text{in} \quad Y_1 \leqslant Y \leqslant Y_0, \qquad (5.4.2b)$$

$$\left.\begin{aligned} Y_s &= Y_1 \\ \xi &= Y - Y_1 \\ H &= 0 \\ \xi_0 &= 0 \end{aligned}\right\} \quad \text{in} \quad Y_0 \leqslant Y_1. \qquad (5.4.2c)$$

The wavenumbers and frequencies for the resonant triad used in this calculation are given approximately by

$$\left.\begin{aligned} (k_1, \omega_1) &= (-2.592, 0.5292) \\ (k_2, \omega_2) &= (1.15, -0.3819) \\ (k_3, \omega_3) &= (1.442, -0.1473) \end{aligned}\right\}. \qquad (5.4.3a)$$

The corresponding group velocities, which are all negative, are given approximately by

$$\left.\begin{aligned} c_{g_1} &= -0.02 \\ c_{g_2} &= -0.22 \\ c_{g_3} &= -0.08 \end{aligned}\right\}. \qquad (5.4.3b)$$

The interaction coefficients in (5.3.5) and (5.3.6) will be given approximately by

$$\left.\begin{aligned} K_{10} &= -210.8 \\ K_{20} &= 22.03 \\ K_{30} &= 6.818 \end{aligned}\right\}. \qquad (5.4.3c)$$

The topographic parameter σ determined by (5.3.2) is given approximately by

$$\sigma = 0.8206, \qquad (5.4.4)$$

where

$$\left.\begin{aligned} \mu_{10} &= 0.7003 \\ \mu_{20} &= -0.7003 \\ \mu_{30} &= 0.8687 \end{aligned}\right\}. \qquad (5.4.5)$$

For this example we will set

$$\left.\begin{aligned} Y_0 &= -1 \\ Y_1 &= -3 \end{aligned}\right\}. \qquad (5.4.6)$$

The initial values of the envelope amplitudes b_j, and the phase Φ_j will be specified at the position $Y = 0$. We will assume that initially the resonant triad is maximally interacting, with the initial envelope phases given by

$$\left.\begin{aligned} \Phi_1(0) &= \pi/2 \\ \Phi_2(0) &= 0 \\ \Phi_3(0) &= 0 \end{aligned}\right\}. \qquad (5.4.7)$$

The wavelength of the wave–wave interaction (i.e., the distance Y over which the energy exchange goes through one complete cycle) is determined by the roots

of the cubic potential, which in turn depend in part on the wave initial amplitudes. For the simulation described here, we have chosen the initial conditions

$$\left.\begin{aligned} b_1(0) &= 1.0 \\ b_2(0) &= 0.0029 \\ b_3(0) &= 0.0010 \end{aligned}\right\}, \qquad (5.4.8)$$

for the real amplitudes determined by (5.3.5). These initial values imply that the interaction nondimensional wavelength in the absence of alongshore topography is about one nondimensional Y unit. Note that $b_1(0)$ is assumed to be relatively large compared to $b_2(0)$ and $b_3(0)$. We have chosen these initial conditions because Hsieh and Mysak interpreted the triad observed by Cutchin and Smith as corresponding to the interaction of a relatively large amplitude atmospherically generated shelf wave with two relatively small amplitude shelf waves.

In Fig. 6, we show the energy cycle from $Y = 0.0$ to $Y = -5.0$ in the absence of any alongshore topography (i.e., $\bar{H} = 0$). The relative envelope amplitude magnitudes reflect the energy partition between the members of the triad as a function of position along the coast at a particular moment in time. Since the group velocity is negative for all members of the triad, it may be useful to think of the energy as starting at $Y = 0.0$ and progressing to $Y = -5.0$. We can see that for the first half of the cycle, for example, $-0.5 \leqslant Y \leqslant 0.0$, the energy is extracted from wave 1 (the wave with the interaction coefficient with a sign opposite the other two) and transferred to waves 1 and 3. For the second half of the cycle, for example, $-0.1 \leqslant Y \leqslant -0.5$, the process is reversed and the energy is transferred back to wave 1 from waves 2 and 3. In the absence of any alongshore topography the flow of energy among the members of the triad pulsates indefinitely with a fixed spatial/temporal period.

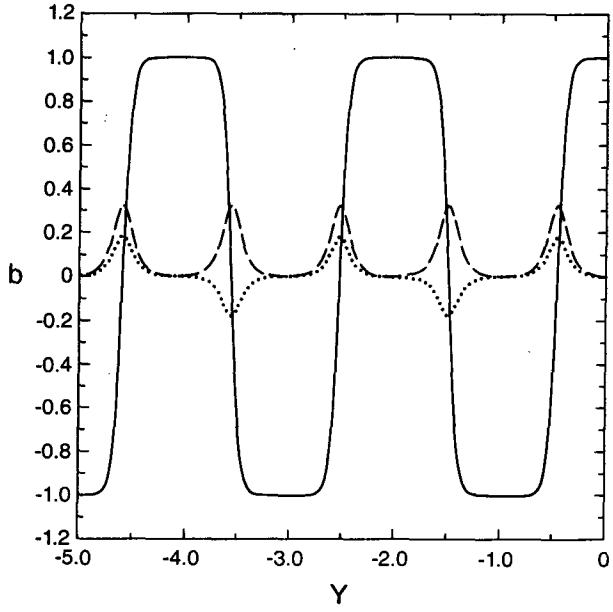

FIG. 6. Plot of b_j versus Y for the initial amplitudes given by (5.4.8) with no topographic anomaly. Wave 1, wave 2, and wave 3 are denoted by the solid, dashed, and dotted lines, respectively.

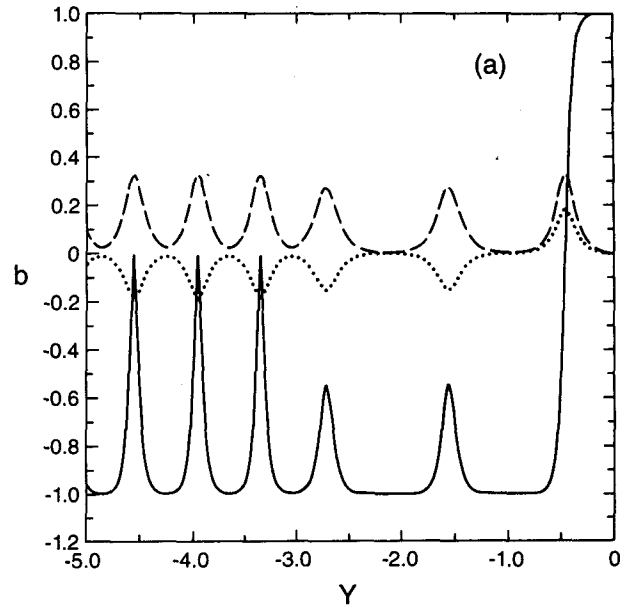

FIG. 7a. Plot of b_j versus Y for $H = 0.5$, $Y_0 = -1.0$, and $Y_1 = -3.0$.

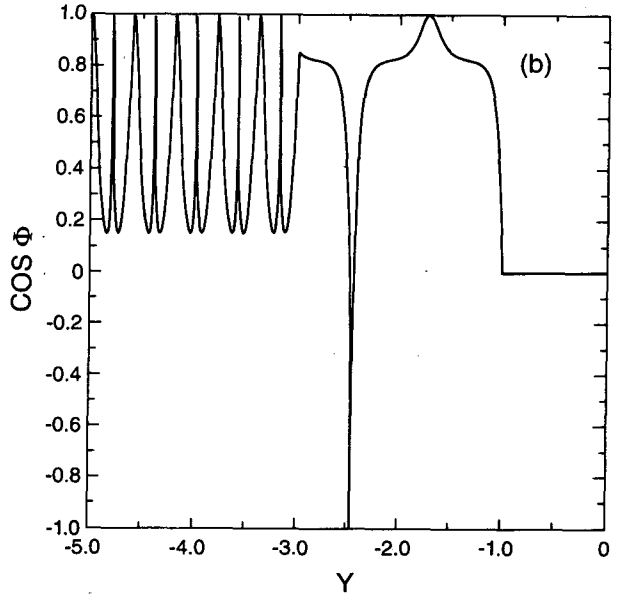

FIG. 7b. Plot of $\cos(\Phi)$ versus Y for the parameter values given in Fig. 7a. Maximum energy exchange occurs when $\cos(\Phi) = 0$, and no energy exchange occurs when $\cos(\Phi) = \pm 1$.

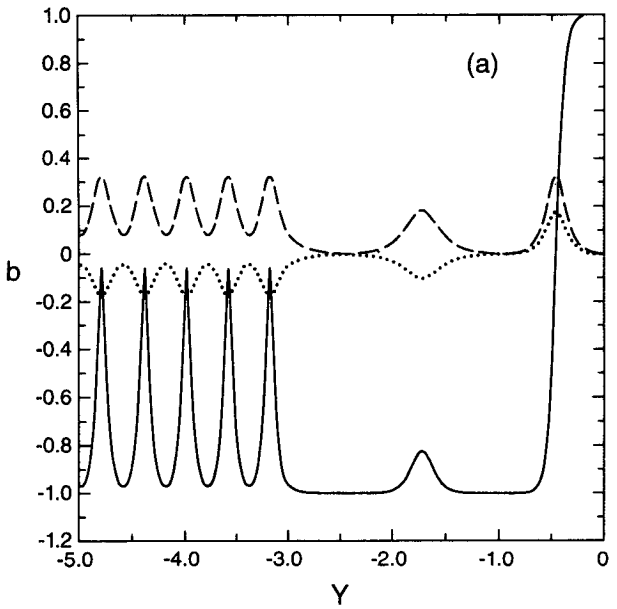

FIG. 8a. Plot of b_j versus Y for a moderate topographic height of $H = 0.75$ with Y_0 and Y_1 given in Fig. 7a.

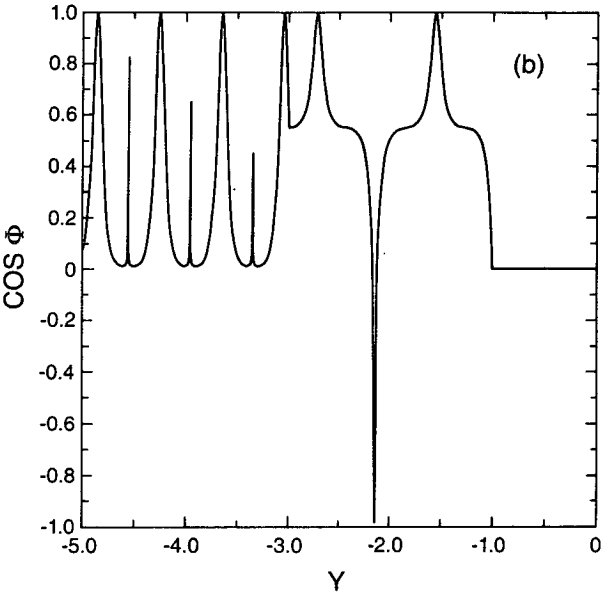

FIG. 8b. Plot of $\cos(\Phi)$ versus Y for the parameter values given in Fig. 8a. Maximum energy exchange occurs when $\cos(\Phi) = 0$, and no energy exchange occurs when $\cos(\Phi) = \pm 1$.

In Figure 7 we show how the energy exchange is modified for a "small" topographic jump parameter of $\bar{H} = 0.5$. In the initial region where the water depth has not yet changed, $-1.0 < Y < 0.0$, the energy exchange is unforced and is identical to that depicted in Fig. 6. However, over the region where the water depth has changed $-3.0 < Y < -1.0$, the energy partition has been modified; see Fig. 7a. While energy exchange still occurs, it does so in a less complete fashion in that the magnitude of the amplitude of wave 1 never decreases to zero while the maximum values of the amplitudes of waves 2 and 3 are reduced. Also, the effective wavelength of energy exchange over the topographic feature has been increased to about 1.2 units. Once the topographic feature has been traversed ($Y \leqslant -3.0$), the energy exchange nearly returns to its pretopographic level, although the wavelength of interaction is greatly reduced. That the energy exchange nearly returns to its pretopographic level in the post-topographic region is not, however, a property that holds generally but depends on the particular length and height of the topographic feature.

It follows from (5.3.5) and (5.3.6) that the topographically induced dephasing and resulting reduction in the efficiency of the energy exchange is determined by the magnitude of $\cos[\Phi(Y)]$ [or equivalently $\sin(\Phi)$]. If $\cos(\Phi) = 0$, it follows that maximum energy exchange is occurring. If $|\cos(\Phi)| = 1$, then there is no energy exchange. Figure 7b is a plot of $\cos(\Phi)$ versus Y for $\bar{H} = 0.5$. In the initial no-topography region $-1.0 < Y < 0.0$, we have $\cos(\Phi) = 0$ and hence maximum energy exchange is occurring. However, over the region of nonzero topography $-3.0 < Y < -1.0$, $\cos(\Phi)$ begins to fluctuate between the value of $+1.0$ and -1.0. This change in Φ is caused by the forcing due to the nonzero jump parameter ($\bar{H} \neq 0$). Moreover, we can see that even after the topography has been traversed $\cos(\Phi(Y)) \neq 0$ so that the wave–wave energy exchange remains permanently suppressed.

One can see how the magnitude of $\bar{H}$ affects the energy exchange over the topography and even in the posttopographic region by looking at Fig. 8, where $\bar{H}$ is increased to the value of 0.75. We can see in Fig. 8a that over the topographic feature, the increase in $\bar{H}$ further decreases the wave–wave energy exchange and that the wavelength of the interaction is increased to about 1.4 nondimensional units. Here, again, we see in Fig. 8b that in the post-topographic region the wave–wave energy exchange remains suppressed.

If we backtrack through transformations (5.3.4), (2.31), and (2.15), we can write the expressions for the individual streamfunctions in the form

$$\left.\begin{aligned}
\psi_1^{(0)} &= b_1(\varepsilon y)\phi(x)\exp[i(\theta_1 \\
&\quad + \mu_{1_0}h_1(Y)/c_{g_1} + \Phi_1(Y))] + \text{c.c.} \\
\psi_2^{(0)} &= b_2(\varepsilon y)\phi(x)\exp[i(\theta_2 \\
&\quad + \mu_{2_0}h_1(Y)/c_{g_2} + \Phi_2(Y))] + \text{c.c.} \\
\psi_3^{(0)} &= b_3(\varepsilon y)\phi(x)\exp[i(\theta_3 \\
&\quad + \mu_{3_0}h_1(Y)/c_{g_3} + \Phi_3(Y))] + \text{c.c.}
\end{aligned}\right\}, \tag{5.4.9}$$

where θ_j, ($j = 1, 2, 3$), is the "fast" phase variable given by $k_j y - \omega_j t$. If we think of (5.4.9) as a plane wave solution, as in WKB theory, we can identify the total phase of the jth wave as

$$\Theta_j = \theta_j - \mu_{j_0} h_1(Y)/c_{g_j} + \Phi_j(Y), \quad (5.4.10)$$

from which we can identify in turn the wavenumber denoted by $\kappa_j(\varepsilon y)$, as given by

$$\kappa_j = \partial\Theta_j/\partial y$$

$$= k_j + \varepsilon[\partial\Phi_j/\partial Y - \mu_{j_0} h_1'(Y)/c_{g_j}] \quad (5.4.11)$$

for $j = 1$, 2, and 3. If we now form the quantity $\kappa_1 + \kappa_2 + \kappa_3$, it follows, upon using the resonance conditions and the definition of $\Phi(Y)$, that

$$\sum_{j=1}^{3} \kappa_j = \varepsilon\Phi_Y. \quad (5.4.12)$$

Thus, the resonance condition applied to the complete WKB wavenumber is no longer satisfied if $\Phi_Y \neq 0$. We can interpret $\varepsilon\Phi_Y$ in (5.4.12) as a topographically induced wavenumber mismatch.

6. Summary and discussion

In this paper, we have attempted to develop a theory to describe the Ekman damping and topographic modulation of resonantly interacting continental shelf waves. The resonant interaction equations were derived by using a multiple-scale asymptotic expansion in which it was assumed that 1) the e-folding time due to the Ekman friction was comparable to the time of energy transfer due to the nonlinear resonant interaction, and that 2) the alongshore topography varied over the same length scale as the energy exchange process. This expansion resulted in a set of evolution equations for the wave packet amplitudes including the effects of alongshore topography and bottom friction.

The damping coefficient for each wave in the governing equations was found to be inversely proportional to the phase speed. The very short shelf waves (lengths $\sim$ 100–140 km), predicted by the triad theory for the Oregon shelf would have very small phase speeds and would thus be quickly dissipated by bottom friction as suggested by Hsieh and Mysak.

We have shown that in the absence of damping the forced wave interaction equations conserved energy. To isolate on the one hand the balance between dissipation and nonlinear energy exchange, and on the other the effect of topographic forcing on the resonant interactions, we looked at the purely temporal and the steady-state problems separately.

The purely temporal problem with bottom friction in the absence of alongshore topographic variation was numerically solved. Because estimates for the vertical eddy viscosity vary considerably, it is difficult to assess the exact effect of bottom friction. For lower estimates of the friction parameter, the frictional decay time scale is long enough that energy exchange due to wave–wave interactions may still be of importance. For the upper estimates of Ekman friction, dissipative losses overshadow any energy exchange due to resonant wave–wave interactions.

An exact nonlinear solution to the steady-state wave–wave interaction equations in the absence of bottom friction and forced by a linearly varying topographic coefficient was presented. These solutions were expressed in terms of Jacobi elliptic functions. In section 5.d we showed how the solutions of 5.c can be pieced together to construct a solution for a resonant triad of waves forced by a piecewise constant topographic bump. Even though this topographic anomaly is very crude, the solutions were able to describe, at least qualitatively, the mechanism by which topographic forcing acts to "dephase" a resonant triad.

The effect of alongshore topography variation is to inhibit nonlinear energy exchange between the members of the triad. We have shown that the effect of topographic forcing is to induce a dephasing of the resonant triad which is then permanently maintained by the wave–wave interaction. The dephasing can be interpreted as a small amplitude slow-varying oscillation in the alongshore wavenumbers. The individual envelope phase functions will not, in general, satisfy the triad resonance conditions in the presence of topography or after the topographic feature has been traversed, and this in turn can be interpreted as responsible for the suppression of the energy exchange between the waves. Another important effect is that the wavelength or period of the exchange cycle is modified in both the topographic region and the posttopographic region. The degree to which the energy exchange is reduced depends on the height of the topographic feature, the initial envelope amplitudes and the length of the topographic feature.

Several shortcomings remain to our model. Stratification and atmospheric forcing have yet to be included in the model. Atmospheric forcing in particular, must probably be included to compensate for the large dissipation in energy if resonant interactions are to be expected to explain the transfer of a significant amount of energy to the other members of the triad. One important drawback is that the interactions that we have examined have been in the main steady. As a result we have not examined in any real detail the initial-value problem for the topographically forced interactions of continental shelf waves. This would be especially interesting since the resonant triad used by Hsieh and Mysak (1980) was inherently time dependent; that is, the group velocities were not all of the same in sign. A numerical study with a more realistic topographic configuration would also be very interesting.

Acknowledgments. Preparation of this manuscript was supported in part by grants awarded to G.E.S. by the Natural Sciences and Engineering Research Council of Canada and by the Department of Fisheries and Oceans of Canada. F.W.P. expresses his thanks for a

Teaching Assistantship awarded by the Department of Mathematics and held during the period this work was completed.

REFERENCES

Abramowitz, M., and J. A. Stegun, 1965: *Handbook of Mathematical Functions.* Dover, 1046 pp.

Adams, J. K., and V. T. Buchwald, 1969: The generation of continental shelf waves. *J. Fluid Mech.*, **35,** 815–826.

Boyce, W. E., and R. C. DiPrima, 1969: *Elementary Differential Equations and Boundary Value Problems.* 2d ed. Wiley, 582 pp.

Buchwald, V. T., and J. K. Adams, 1968: The propagation of continental shelf waves. *Proc. Roy. Soc. London,* **A305,** 235–250.

Craik, A. D. D., 1985: *Wave Interactions and Fluid Flows.* Cambridge University Press, 332 pp.

Cree, W., and G. E. Swaters, 1991: On the topographic dephasing and amplitude modulation of nonlinear Rossby wave interactions. *Geophys. Astrophys. Fluid Dyn.*, **61,** 67–99.

Cutchin, D. L., and R. L. Smith, 1973: Continental shelf waves: Low-frequency variations in sea level and currents over the Oregon continental shelf. *J. Phys. Oceanogr.*, **3,** 73–82.

Hsieh, W. W., and L. A. Mysak, 1980: Resonant interactions between shelf waves, with applications to the Oregon Shelf. *J. Phys. Oceanogr.*, **10,** 1729–1741.

Huyer, A. B., M. Hickey, J. D. Smith, R. L. Smith, and R. D. Pillsbury, 1975: Alongshore coherence at low frequency in currents observed over the continental shelf off Oregon and Washington. *J. Geophys. Res.*, **80,** 3495–3505.

Kaup, D. J., and A. C. Newell, 1978: Solitons as particles, oscillators, and in slowly changing media: A singular perturbation theory. *Proc. Roy. Soc. London,* **A361,** 413–446.

——, A. Reimann, and A. Bers, 1979: Space–time evolution of nonlinear three-wave interactions: I. Interactions in homogeneous medium. *Rev. Mod. Phys.*, **51,** 275–310.

Meacham, S., 1988: Non-modal baroclinic instability. *Dyn. Atmos. Oceans,* **12,** 19–45.

Pedlosky, J., 1987: *Geophysical Fluid Dynamics.* Springer-Verlag, 710 pp.

Primeau, F. W., 1992: The effect of alongshore topographic variation and bottom friction on shelf wave interactions. M.S. thesis, Department of Mathematics, University of Alberta, 118 pp.

Weiland, J., and H. Wilhelmsson, 1977: *Coherent Nonlinear Interactions of Waves in Plasmas.* Pergamon, 353 pp.